 FDMP, vol.5, no.3, pp.261-282, 2009

Some Benchmarks of a Side Wall Heated Cavity Using Lattice Boltzmann Approach

R. Djebali[1,2], M. El Ganaoui[2,3], H. Sammouda[1] and R. Bennacer[4]

Abstract: The simplified thermal lattice Boltzmann model (STLBM) developed by Peng, Shu and Chew (2003) is used in this work to simulate low-Rayleigh-number natural convection in a heated rectangular cavity on a uniform grid. It is shown how by resorting to the double populations approach both hydrodynamic and thermal fields can be effectively simulated. Furthermore, a general benchmark is carried out to account for the effect of different parameters in relatively wide ranges. Results are compared with previous works available in the literature.

Keywords: Lattice Boltzmann method, natural convection, heated cavity, benchmark solution, secondary parameters, low Rayleigh numbers.

Nomenclature

a	order of accuracy of the model
Ra	$g\beta\Delta TH^3/(\nu\chi)$ Rayleigh number
b	power of the law $Nu \propto (Ra)^b$
T	fluid temperature
c	$\delta x/\delta t$ lattice streaming speed
T_h, T_c	temperatures of hot and cold walls
c_s	$c/\sqrt{3}$ lattice sound speed
T_r	reference temperature
$\vec{e}_\alpha$	discrete velocity in α direction
$\vec{V}$	(u,v) velocity vector
f_α, θ_α	discrete distribution functions for density and internal energy
W	width of the enclosure
$f_\alpha^{eq}, \theta_\alpha^{eq}$	equilibrium density and internal energy distribution functions

[1] LETTM, Univ. Tunis EL Manar, Tunisia
[2] SPCTS, Univ. Limoges, France
[3] ganaoui@unilim.fr
[4] LEEVAM, Univ. Cergy-Pontoise, France

U	$\sqrt{g\beta\Delta TH}$ velocity scale for natural convection
F_α	Source term
ΔT	$T_h - T_c$ horizontal temperature difference
$\vec{g}$	gravity field
n	Number of nodes
p	ρc_s^2 ideal gas pressure
t	time
$\vec{x}$	(x,y) lattice coordinates
δt	time step
$u_{\max}, v_{\max}$	maximum velocity at mid-width and mid-height
δx, δy	lattice spacing units
Ar	W/H aspect-ratio
C	constant of the power relation-ship
D	space dimension
E	relative error
$\vec{G}$	$-\beta(T-T_r)\vec{g}$ buoyancy force per unit mass
H	height of the enclosure
$\overline{Nu}$	$1+\langle u.T\rangle/(\chi.\Delta T/W)$ average Nusselt number
Nu_0	Nusselt number at the hot wall
Ma	$\left\|\vec{V}\right\|/c_s$ mach number
Pr	v/χ Prandtl number
R	gas constant

Greek symbols

ω_α	weights for the particle equilibrium distribution function
ρ	$\sum_\alpha f_\alpha$ fluid density
ρ_r	reference fluid density
δ	small parameter (Knudsen number)
υ	kinetic viscosity
ε	$DRT/2$ internal energy
χ	thermal diffusivity
β	thermal coefficient expansion
γ	the cavity inclination angle
τ_υ, τ_c	relaxation times
$\nabla.$	divergence operator
∇	gradient operator

Subscripts Suscripts

eq	equilibrium
i	index
neq	non-equilibrium part
max	maximum
CFL	Courant-Frediric-Lewy stability condition

1 Introduction

The socalled lattice Boltzmann method (LBM) derives from the lattice Boltzmann equation and basically relies on a discrete distribution function representing the probability of finding particles with a certain range of velocities at certain range of locations at a given time (Succi (2001), Sukop et al. (2005), Mohamad (2007)). This new alternative approach has proved its ability to simulate large variety of fluid flows.

In other words, the simulation of the fluid flows by using the lattice Boltzmann equation (LBE) method is based on kinetic equations and statistical physics, unlike conventional methods that are based on continuum mechanics.

In practice, the advantage of the LBM relies in its stability (unconditionally stable) and the linear form of its scheme (algebraic operations), which overcome the well-known CFL stability condition and the drawback of the non-linear form of the Navier-Stokes equations (which leads generally to algebraic equations). For its efficiency and accuracy, the LBM has received recently considerable attention by fluid dynamic researchers (Zou and He (1997), Chen and Doolen (1998), Guo and Zheng (2002), Shu and Peng (2002-2005) and Semma, El Ganaoui and Bennacer (2007-2008)).

It is also worth pointing out that the LBE is the minimal form of the BE and that it can recover the hydrodynamic and thermal behaviours at the macroscopic level (mass, momentum and energy conservation) in second order of accuracy in time and space. The quality of the computational efficiency and accuracy of the LBM reside on its ability to model complicated flows such as multiphase flows, chemically reacting flows (Yamamoto, Takada, Misawa (2005)), micro-flows (Chew, Niu and Shu (2006)) in 2D and 3D isothermal and thermal flows (Bouzidi, D'Humières, Lallemand (2001), D'Humières, Bouzidi, Lallemand (2001)) on uniform and non uniform grid. Massaioli, Benzi, and Succi (1993) have developed first the thermal LB model and now there are three thermal LB models: The multi-speed approach (Chen and Doolen (1998)), the passive scalar approach (D'Orazio, Corcione and Cielata (2004)) and the double population approach (He and Luo (1998)). This

new approach has proved the ability to simulate large variety of fluid flows and to handle complex geometries (Bouzidi, Firdaouss and Lallemand (2001), Lallemand and Luo (2003)) and has expressed a flexibility to be coupled with traditional CFD method (Mezrhab, Bouzidi and Lallemand (2004)).

An extension of the passive-scalar thermal model, where viscous and compressive heating are neglected, was recently proposed by introducing the internal energy density distribution function (IEDDF model). So, the omitting of the viscous heat dissipation and compression work done by pressure in macroscopic energy equation can be reflected by dropping out the gradient term in the evolution equation for the new distribution function, since such gradient term is mainly used to recover these terms through the Chapman-Enskog expansion. Following the work of Peng, Shu and Chew (2003) a simplified thermal distribution model is proposed. This model was proved to fully recover the energy equation at the macroscopic level incorporating future work and heat dissipation correctly.

At this stage, let us notice that natural convection in heated square cavity is not only an ideal case for testing numerical models intended for the resolution of Navier-Stokes equations, but it has also extensive background applications in many fields such as aeronautics and electronics.

For instance the heating-from-below condition provides an important test case for instable flows occurring in crystal growth (El Ganaoui and Bontoux (1998), El Ganaoui (2002), El Ganaoui and Prud'homme (2004), Lappa (2007)).

The case insulated from below and above with vertical walls maintained at a fixed temperature is encountered for problems dealing with heat transfer in buildings; it is also relevant to solar energy collectors and double glazed windows.

These fields were the subject of numerous comprehensive studies using the LB approach to understand the natural convection phenomena (Jami, Mezrhab, Bouzidi and Lallemand (2007), Jami, Amraqui, Mezrhab and Abid (2008), Mezrhab, Jami, Abid, Bouzidi and Lallemand (2006)) and their interaction with radiation (Mezrhab, Jami, Bouzidi and Lallemand (2007), Mezrhab, Moussaoui and Naji (2008), Bouali, Mezrhab, Amaoui, Bouzidi (2006)).

It is known that several parameters can influence the dynamic and thermal behaviours within a heated cavity. The effect of the Rayleigh number, as a controlling parameter of convection, was studied by many authors for heated square cavity case (de Gassowski, Xin and Daube (2003)); a symmetry breaking phenomenon was underlined under 3D approach by Bennacer et al. (2006). Various numerical simulations have been performed to study the major effects of the different parameters (Prandtl number, the orientation of the cavity and the aspect ratio ($Ar=W/H$: width/height)) on the structure of the flow, but few studies have been conducted

using LBM.

The purpose of this work is to validate such model through its application to the configuration of differentially heated square cavity (horizontal temperature gradient, see Fig.1) as well as to establish a general benchmark reproducing existing results for the effect of each parameter. The present study investigates also the mutual effects on the heat transfer expressed by the Nusselt number; some correlations will be therefore established in a wide range of the Rayleigh number ($10^3 \leq Ra \leq 10^6$), the Prandtl number($0.025 \leq Pr \leq 6$), the inclination of the cavity ($0^\circ \leq \gamma \leq 270^\circ$) and the aspect-ratio ($1/8 \leq Ar \leq 8$). The fluid is assumed to be incompressible, the Boussinesq approximation is assumed to be valid and the radiation effects is neglected.

The remaining part of the paper is organized as follows. Section 2 introduces the simplified thermal lattice Boltzmann model in the presence of the buoyancy force. Dimensionless parameters and implementation of boundary conditions are also presented. Section 3 presents a validation of the model through its application the dynamics and thermal behavior in a differentially heated air-filled square cavity. Order of accuracy of the model is demonstrated. In section 4, the effects of a quite large number of secondary parameters linked to fluid, configuration and orientation are studied separately at first and then coupled.

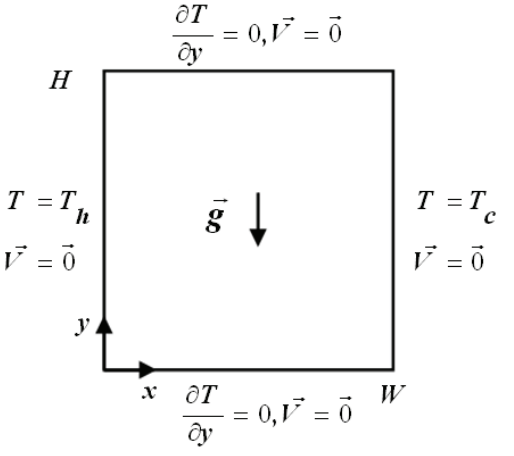

Figure 1: Schematic geometry for natural convection in a square cavity.

2 The 2D incompressible simplified thermal lattice Boltzmann model

This part is devoted to the general ideas of the STLBM whose details can be found in Peng, Shu and Chew (2003). The considered assumptions are: the BGK approximation (single relaxation time) and incompressible flow (low Mach number).

2.1 Lattice Boltzmann hydrodynamics model

Fig.2 presents the nine-velocity LBM model on a 2D square lattice, denoted D2Q9 model. We use this model for the current study. Let δx and δy be the distance a particle move of grid spacing and $c = \delta x/\delta t$ be the lattice streaming speed.

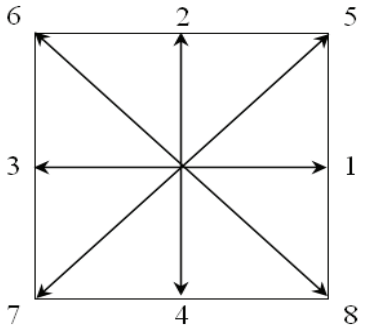

Figure 2: The nine-velocity LBM model on 2D square lattice.

The discrete velocities of the D2Q9 model are defined as follows

$$\begin{cases} \vec{e}_\alpha = (0,0), & \alpha = 0, \text{ rest particle} \\ \vec{e}_\alpha = (\pm c, 0), & \alpha = 1,2,3,4 \\ \vec{e}_\alpha = (\pm c, \pm c), & \alpha = 5,6,7,8 \end{cases}$$

The governing equation for the density distribution function is

$$f_\alpha(\vec{x}+\vec{e}_\alpha \delta t, t+\delta t) - f_\alpha(\vec{x},t) = -\frac{1}{\tau_\upsilon}[f_\alpha(\vec{x},t) - f_\alpha^{eq}(\vec{x},t)] + \delta t F_\alpha \tag{1}$$

where τ_υ characterizes the relaxation time resulting from the BGK approximation for the collision operator, and the equilibrium density distribution function is given as

$$f_\alpha^{eq} = \omega_\alpha \rho \left[1 + 3\frac{\vec{e}_\alpha.\vec{V}}{c^2} + \frac{9}{2}\frac{(\vec{e}_\alpha.\vec{V})^2}{c^4} - \frac{3}{2}\frac{\vec{V}^2}{c^4}\right] \tag{2}$$

where $w_0 = 4/9$, $w_\alpha = 1/9$ for $\alpha = 1,2,3,4$ $w_\alpha = 1/36$ for $\alpha = 5,6,7,8$ and $\vec{V} = (u,v)$.

The macroscopic density and velocity are calculated by

$$\rho = \sum_\alpha f_\alpha \tag{3}$$

$$\rho\vec{V} = \sum_\alpha \vec{e}_\alpha f_\alpha \tag{4}$$

The continuity and Navier-Stokes equation can be recovered through the Chapman-Enskog expansion (He and Luo (1997)) whose the derivation details will not be shown here. The final results of the continuity and Navier-Stokes equation are

$$\partial_t \rho + \nabla.(\rho\vec{V}) = O(\delta^2) \tag{5}$$

$$\partial_t(\rho\vec{V}) + \nabla.(\rho\vec{V}\vec{V}) = -\nabla p + \upsilon[\nabla^2(\rho\vec{V}) + \nabla(\nabla.(\rho\vec{V}))] + O(\delta^2) \tag{6}$$

where δ is a small parameter proportion to the Knudsen number (the ratio of the mean free path to a characteristic flow length), $p = \rho c_s^2$ is the pressure from the equation of the state for the ideal gas, $c_s = c/\sqrt{3}$ is the sound speed and the kinetic viscosity is given by

$$\upsilon = \frac{(2\tau_\upsilon - 1)}{6}\frac{(\delta x)^2}{\delta t} \tag{7}$$

The assumption of low Mach number ($Ma = \left\|\vec{V}\right\|/c_s << 1$) invoked as the nearly incompressible limit is approached, and then the continuity and Navier-Stokes equations will be expressed as

$$\nabla.(\vec{V}) = O(\delta^2) \tag{8}$$

$$\partial_t\vec{V} + \vec{V}.\nabla\vec{V} = -\frac{\nabla p}{\rho} + \upsilon\nabla^2\vec{V} + O(\delta^2) \tag{9}$$

2.2 Lattice Boltzmann thermal model

Following the works of Peng, Shu and Chew (2003) the simplified thermal model does not include complex gradient terms; accordingly, it keeps the simple form as the isothermal LBM and allows the use of the bounce back rule of the non-equilibrium distribution function for the boundary conditions. For these considerations we decide to use this model.

The governing equation for the simplified energy distribution model is

$$\theta_\alpha(\vec{x}+\vec{e}_\alpha\delta t, t+\delta t)-\theta_\alpha(\vec{x},t)=-\frac{1}{\tau_c}[\theta_\alpha(\vec{x},t)-\theta_\alpha^{eq}(\vec{x},t)] \tag{10}$$

The corresponding equilibrium energy distribution function following the work of He, Chen and Doolen (1998) is

$$\theta_\alpha^{eq}=\omega_\alpha\rho\varepsilon\left[\frac{3(\vec{e}_\alpha^2-\vec{V}^2)}{2c^2}+3\left(\frac{3\vec{e}_\alpha^2}{2c^2}-1\right)\frac{(\vec{e}_\alpha.\vec{V})}{c^2}+\frac{9}{2}\frac{(\vec{e}_\alpha.\vec{V})^2}{c^4}\right] \tag{11}$$

where $\varepsilon = DRT/2$, R is the gas constant and D is the space dimension. Then the macroscopic temperature is calculated by

$$\rho\varepsilon=\sum_\alpha\theta_\alpha \tag{12}$$

This thermal energy distribution function can recover the macroscopic energy equation by using the Chapman-Enskog expansion technique; the final result is as below:

$$\partial_t(\rho\varepsilon)+\nabla.(\rho\vec{V}\varepsilon)=\chi\nabla^2(\rho\varepsilon)+O(Ma^2\delta T) \tag{13}$$

and the formula of the diffusivity χ is written as

$$\chi=\frac{1}{3}(2\tau_c-1)\frac{(\delta x)^2}{\delta t} \tag{14}$$

2.3 Buoyancy force and dimensionless parameters

In simulating natural convection problem, the additional body force term,F_α, can be formulated by the Boussinesq approximation. The Boussinesq approximation considers that all the properties of the fluid are constant, except the fluid density given by $\rho=\rho_r(1-\beta(T-T_r))$, where ρ_r is a reference fluid density, β is the thermal coefficient expansion of the fluid andT_r is a reference fluid temperature, then the external buoyant force $\rho_r\vec{G}=-\rho_r\beta(T-T_r)\vec{g}$ appearing in Navier-stokes equations will be expressed in equation (1) as

$$F_\alpha=\frac{\vec{G}.(\vec{c}_\alpha-\vec{V})}{c_s^2}f_\alpha^{eq} \tag{15}$$

Following these considerations $\left\|\vec{V}\right\| \ll c_\alpha$, $f_\alpha^{eq}\approx w_\alpha\rho(x,t)$, and $T_r=0$, the final form of the external body force is

$$F_\alpha=-3w_\alpha\rho(\vec{x},t)\beta T(\vec{x},t)\vec{g}.\vec{c}_\alpha \tag{16}$$

Natural convection problems are characterized by a characteristic velocity $U = \sqrt{g\beta\Delta TH}$, the kinetic viscosity ν and the thermal diffusivity χ, and then the Prandtl number is defined as

$$Pr = \nu/\chi \tag{17}$$

using the equation (7) and (14) we obtain

$$Pr = \frac{1}{2}\frac{2\tau_\upsilon - 1}{2\tau_c - 1} \tag{18}$$

The Rayleigh number is defined as

$$Ra = \frac{g\beta\Delta TH^3}{\nu\chi} \tag{19}$$

The average Nusselt number, $\overline{Nu}$, is estimated to investigate the enhancement of the thermal transfer. $\overline{Nu}$ is defined as

$$\overline{Nu} = 1 + \frac{\langle u.T\rangle}{\chi.\Delta T/W} \tag{20}$$

where $\Delta T = 1$ and $\langle\rangle$ denotes the average value throughout the domain.

The average Nusselt number at the hot wall, Nu_0, is calculated using a second order finite difference scheme as

$$Nu_0 = \sum_{j=0}^{n} \frac{3T_{0,j} - 4T_{1,j} + T_{2,j}}{2} \tag{21}$$

2.4 Implementation of the boundary conditions

The bounce-back rule of the non-equilibrium distribution function proposed by Zou and He (1997) is used for the boundary condition. The density distribution function at the boundary should satisfy the following condition:

$$f_\alpha^{neq} = f_\beta^{neq} \tag{22}$$

where $\vec{e}_\alpha$ and $\vec{e}_\beta$ have opposite directions. The energy distribution function at the boundary satisfies

$$g_\alpha^{neq} - \vec{e}_\alpha^2 f_\alpha^{neq} = -(g_\beta^{neq} - \vec{e}_\beta^2 f_\beta^{neq}) \tag{23}$$

The wall temperatures are used for the calculation of the internal energy equilibrium functions.

3 Validation of the LB model using 2D square cavity

3.1 Grid independence

In the simulations, the 2D cavity is mapped using a square lattice, where $\delta x = \delta y$ for the D2Q9 model. The aspect ratio $Ar = W/H$ is equal to the unit. The Prandtl number is assumed to be constant with a value 0.71 and the Rayleigh number is chosen to be 10^4.

Grid independence is examined using several different grid systems quite coarser than that chosen by Peng, Shu and Chew (2003), i.e. from 33^2 to 225^2.

Tab. 1 shows numerical solutions of the maximum horizontal velocity at the mid-height and the maximum vertical velocity at the mid-width ($u_{\max}$ and $v_{\max}$ respectively) normalized by the reference velocity χ/H and their locations (y_u and x_v respectively) normalized by the reference length H. The average Nusselt number value $\overline{Nu}$ of the whole of the cavity is also computed.

The relative deviation (error) E of the average Nusselt number from the reference value is defined as

$$E = \left| \frac{\overline{Nu} - \overline{Nu}_r}{\overline{Nu}_r} \right| \tag{24}$$

where $\overline{Nu}_r$ indicates reference results of de Vahl Davis (1983).

The convergence criteria adopted here is defined as

$$\left| \frac{\overline{Nu}(t) - \overline{Nu}(t+5000)}{\overline{Nu}(t)} \right| \leq 10^{-6} \tag{25}$$

In addition, Paolucci and Chennoweth (1989) monitored the oscillations in u, v and T at the location $(x/H, y/H) = (0.1032, 0.8036)$. To show, also, the achievement of steady state we will use the same monitoring point.

In this study we can see that when the number of nodes in each direction increases, the calculated magnitude and location quickly approach the benchmark result, and further more, when the number of nodes increases from 176 to 224, there is not much effect on the result. Hence the results are taken to be grid independent.

3.2 Convergence rate

We suppose the following relationship $E = C.(\Delta x)^a$, here C is a constant, a is the order of accuracy of the model, $\Delta x = 1/n$ and$n$ is the number of nodes for each direction of the square cavity. The results of $ln(E)$ versus $ln(\Delta x)$ are plotted in Fig. 3. The equation of the obtained fitting curve shows that $a \approx 1.95$, then it is obvious

Table 1: Grid dependence in square cavity at Ra=10^4

n	32	80	128	176	224	Davis[a]
u_{max}	16.011	16.1344	16.1593	16.1716	16.1725	16.178
y_u	0.8125	0.825	0.82031	0.8222	0.8227	0.823
v_{max}	19.2777	19.5259	19.5945	19.612	19.618	19.617
x_v	0.1875	0.125	0.11718	0.11666	0.11732	0.119
$\overline{Nu}$	2.1814	2.2255	2.2350	2.240507	2.2417	2.243

that the Nusselt number solution converges at the rate of second order. The slightly distortion via a=2 is due to the bounce-back scheme used at the boundaries (first order accurate).

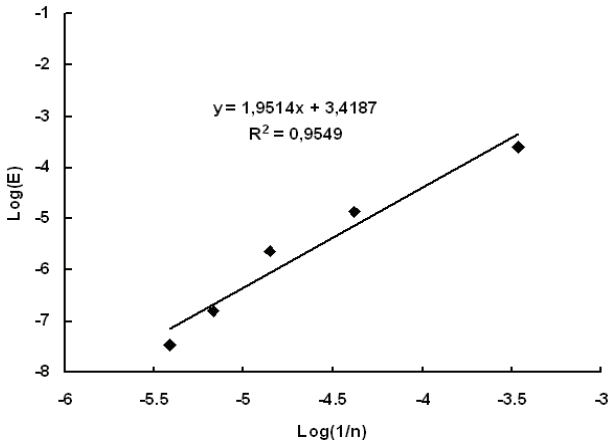

Figure 3: Numerical error versus lattice spacing for square cavity.

3.3 Comparison

Fig. 4 shows the contour maps of the streamlines which shows the flow pattern, the horizontal velocity component, the vertical velocity component and the temperature field for different value of Ra ($Ra = 10^3$, 10^4, 10^5 and 10^6).

These plots agree well with results obtained by Shu and Xue (1998). In addition it is visibly that the property of symmetry which was well studied by de Gassowski, Xin and Daube (2003) is highly shown through the layouts of the streamlines and of temperatures proving that the LBM is able to represent the convection problems with high order of accuracy.

Table 2: Comparison of the present results computed using different grids at different Rayleigh numbers with results of Ref [a]

Ra	Mesh		$u_{max}(y)$	$v_{max}(x)$	Nu_0	$\overline{Nu}$	Error(%)
10^3	32x32	Present	3.618(0.813)	3.659(0.1875)	1.1506	1.1131	0.24
	48x48	Present	3.634(0.813)	3.674(0.1875)	1.138	1.1153	
		Ref [a]	3.649(0.815)	3.698(0.180)	1.117	1.118	
10^4	48 x 48	Present	16.067(0.813)	19.446(0.125)	2.2783	2.2076	0.78
	80 x 80	Present	16.134 (0.825)	19.526(0.125)	2.2647	2.2255	
		Ref [a]	16.190(0.825)	19.638(0.120)	2.238	2.243	
10^5	80 x 80	Present	34.618(0.85)	67.755(0.063)	4.5465	4.4418	0.25
	128 x 128	Present	34.662(0.852)	68.216(0.07)	4.5440	4.5076	
		Ref [a]	34.736(0.855)	68.640(0.065)	4.509	4.519	
10^6	128 x 128	Present	64.265(0.852)	217.145(0.039)	8.7667	8.6372	0.98
	160 x 160	Present	64.414(0.850)	218.343(0.038)	8.8025	8,6931	
	176 x 176	Present	64.511(0.852)	218.281(0.04)	8.8374	8.7134	
		Ref [a]	64.775(0.850)	220.640(0.035)	8.817	8.800	

Ref [a]: de Vahl Davis (1983).

Tab. 2 shows the quantitative comparison. Through these results one can say that the LB results have a very good agreement with those of other methods in both qualitative and quantitative senses. The underlined data indicate the percentage deviation of the current results for $\overline{Nu}$ from de Vahl Davis's results (1983), so the results obtained using the current LB model are consistent. Using a grid size of 128x128 or 176x176, for Ra=10^6, the discrepancy between the two sets of results is less than 0.25% for the four fields u_{max}, v_{max}, $\overline{Nu}$ and Nu_0. Note that in these simulations, we are satisfied by the coarser grid that gives a deviation less than 1%. The maximum relative error is 1.06% obtained for v_{max} at Ra=10^6.

Furthermore, we can observe that the Nusselt number obtained by this model is slightly smaller than the Navier-Stokes result, this is due to the truncated equilibrium distribution function by the so-called low-Mach number approximation $(O(Ma)^2)$.

In confined space many phenomena can be encountered such as plumes, wall jet, thermal boundary layers and viscous boundary layers etc. In the present configuration and for Rayleigh number ranging from 10^3 to 10^4, a circular cellular structure dominates the stream-function field as illustrated in figure Fig.4 (a-d). For higher values of the Rayleigh number, a temperature undershoots and a stationary wave-like structure form, at the up-left and low-right corners where the flow discharges from the thin vertical boundary layer into the core flow. This is due to the fact that high Rayleigh numbers enhance the fluid motion. In addition, the thermal and dynamic boundary layer thicknesses decrease with increasing the Rayleigh number. One can also see the establishing lamellate thermal structure when increasing the Rayleigh number, thus we say that the flow presents a stratified structure. The overshoot and undershoot of the flow patterns between the vertical boundary layers and the core region become more pronounced when Ra increases and will induce a large core region and a divergence of the horizontal wall boundary layers. The main flow is moving along the hot and cold wall and leaves the adiabatic side walls before it reaches isotherm walls.

3.4 Relationship between Nusselt number and Rayleigh number

Previous numerical and experimental investigations of Nusselt number in square cavity showed that the Nusselt number and the Rayleigh number are related by the power law $Nu \propto (Ra)^b$ in which "b" is generally close to 0.3. In the present study, the plots of the best-fitted curves of Nusselt numbers $\overline{Nu}$ and Nu_0 versus the Rayleigh number in the range $10^3 \leq Ra \leq 10^6$ were found to lie along straight lines when plotted as *log(Nu)* versus *log(Ra)* and then, the power relationships $\overline{Nu} = 0.1429Ra^{0.2982}$ and $Nu_0 = 0.1478Ra^{0.2965}$ are obtained. The present correlations are in good agreement with these established by Berkovsky and Polevikov (see

Bennacer et al. (1993-2000)). One can also observe that (for Ar=1) $\overline{Nu} \approx Nu_0$, this is can be explained by the fact that, in steady state, the heat flux given at the hot wall is transferred within the domain and is received at the cold wall. In other hand the exponent of the power law is generally taken between $1/4$ and $1/3$. In this case, we obtain $Nu_0 = 0.0906Ra^{1/3}$ which agrees well with the experimental results of Ozoe and Sayama (1998) where $\overline{Nu} = 0.109Ra^{1/3}$, with a deviation of 0.43% in $Nu_0$for Ra=10^6.

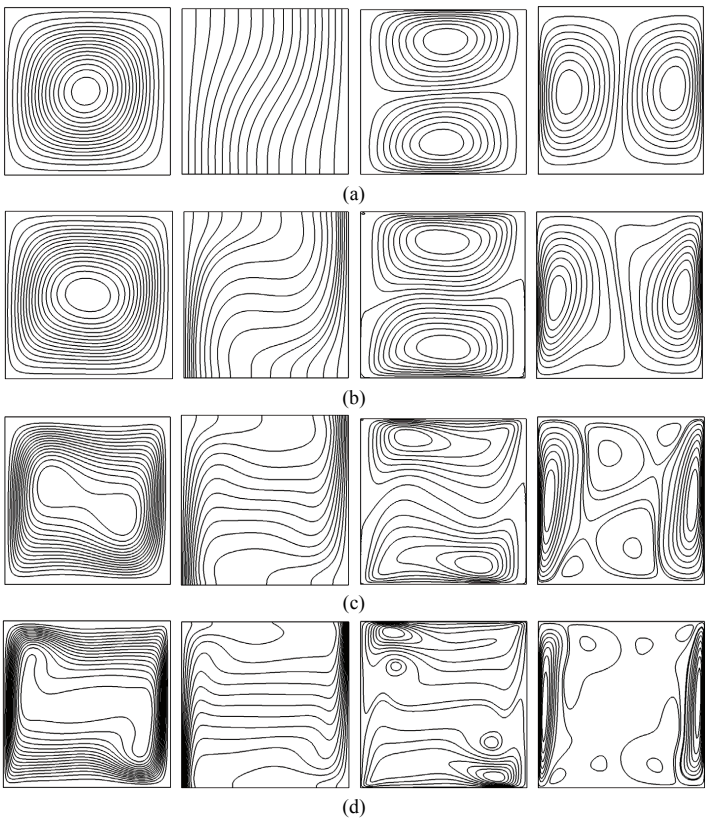

Figure 4: The contour maps of (from left to right) streamlines, temperature, horizontal and vertical velocity components for Ra=10^3 (a), Ra=10^4 (b), Ra=10^5 (c) and Ra=10^6 (d).

4 Effects of the secondary parameters

Several parameters can influence the dynamic and thermal behavior in a differentially heated cavity. We study in this part the effects of the geometry of the cavity,

of its configuration and the effect of the nature of the fluid modeled respectively by the aspect ratio Ar, the angle of inclination of the cavity γ and the Prandtl number Pr. In this section, first we study the effects of these parameters separately, on the left Nusselt number Nu_0, and then we treat the mutual (coupled) effects. The Rayleigh number is chosen to be10^3, 10^4 and 10^5 for all the simulations since the convection mode is preponderant and to be far from instabilities phenomena.

4.1 Effect of the aspect ratio Ar

The effect of the aspect ratio on flow and heat in air-filled cavity has been extensively treated in earlier works (this geometry finds its application in many melting phenomena). When the vertical solid front starts to melt, the aspect ratio W/H increases and one has a *tall/slender* cavity, on the contrary (solidification), one will have a *shallow* cavity. The change of geometry induces the change of critical points, such as the critical Rayleigh, Ra_c, of transitions to time-dependence and chaotic flow.

These transitions occur at broadly different values of Ra, indicating a strong influence of the aspect ratio.

For Ra=10^3 and Ar=0.5 the plot of the temperature field shows a vertical line, then the heat transfer is purely conductive. This can be concluded also from the value of average Nusselt number $\overline{Nu}$ which is close to 1, but $Nu_0 = 2.026$ and increases too with the decrease of Ar. On the contrary when Ar increases (upper to 1) Nu_0 decreases and $\overline{Nu}$ increases excessively, the heat transfer is obviously purely convective. The same behaviour is observed for Ra=10^4 and 10^5. These remarks are in conformity with the results obtained by Ismail and Scalon (2000) or Mohamad et al. (2004).

The plots of Nu_0versus Ra for each aspect ratio are shown in Fig. 5.

The main driving idea of this discussion is to show that there is an aspect ratio ($\approx$0.25) where the Nusselt number is almost independent from the Rayleigh number in this range. Likewise the dependence is strict.

4.2 Effect of the Prandtl number Pr

As discussed above, the heat transfer depends clearly on the aspect ratio. We show here that the nature of the fluid can also affect the heat and the fluid flow. Fig. 6 presents the evolution of the left Nusselt number versus the Prandtl number in the range $0.025 \leq Pr \leq 6$ for different values of the Rayleigh number. One can see that heat transfer decreases when the Prandtl number decreases to reach the value 0.025, which corresponds to the case of liquid metals, such as gallium and mercury. For moderately large values of the Pr (up to 1), the heat transfer pattern remains

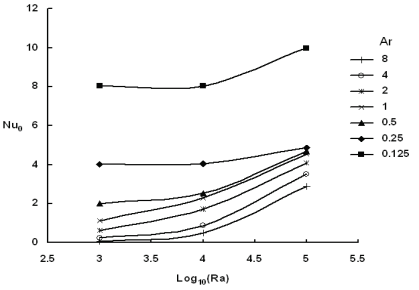

Figure 5: The effect of aspect ratio on heat transfer for $10^3 \leq Ra \leq 10^5$.

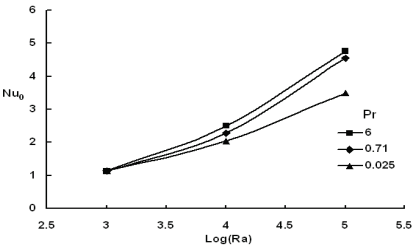

Figure 6: The effect of Prandtl number on heat transfer at various Rayleigh numbers.

relatively unchanged for the three considered values of the Rayleigh number.

4.3 Effect of the angle of inclination γ

The present section illustrates typical results of numerical simulations for various orientations.

Let us recall that only the momentum equation is affected by the change of the angle of inclination (the Boussinesq term). The configuration of an inclined cavity is presented in Fig. 7. The Rayleigh number is chosen to be 10^5. The results show good agreements with previous work in quantitative sense.

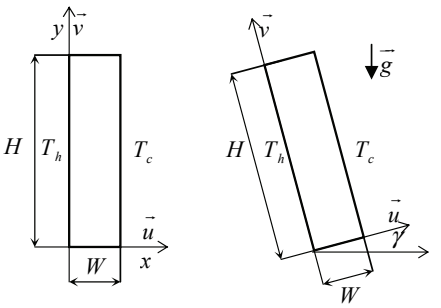

Figure 7: The configuration of the inclined heated cavity.

The results for Ar=1 are plotted in Fig. 8 and are found to reproduce the same profile obtained by Ozoe and Sayama (1975). One can observe that heat transfer increases when the angle γincreases to value close to 15°, the corresponding Nusselt

number being equal to 4.7. With further increasing γ, the value of $\overline{Nu}$ decreases considerably to achieve a minimum at a critical angle between 90° and 100°. The corresponding Nusselt number for the Rayleigh-Bénard of configurationation (90°) is 3.85. When γ increases more, $\overline{Nu}$ increases to exceed the value obtained at $\gamma = 0°$ and certainly to reach again the value 4.7 at $\gamma = 165°$. When γ exceeds 180°, $\overline{Nu}$ decreases clearely to be close to 1 in a configuration of enclosure heated from above ($\gamma = 270°$). This value implies pure diffusive heat transfer. In this configuration, the density of the particle heated at the top wall of the cavity decreases, but the tendency of the particles is to ascend again, thus the agitation will be located at the top, so the whole convective heat decreases.

Rotating the cavity to an angle $\gamma = 90°$leads to the Rayleigh-Bénard configuration. In such case the core region is occupied by one clockwise rotating cell, and the boundary layers are more stretched at the middle of the hot and cold walls. A counter-clockwise cell appears where cold cell starts the hot wall and where hot cell starts the cold one, inducing an increase in $\overline{Nu}$ and probably reveals the way to three-dimensional flow effects and we underline the oscillatory flow obtained for higher *Ra* values.

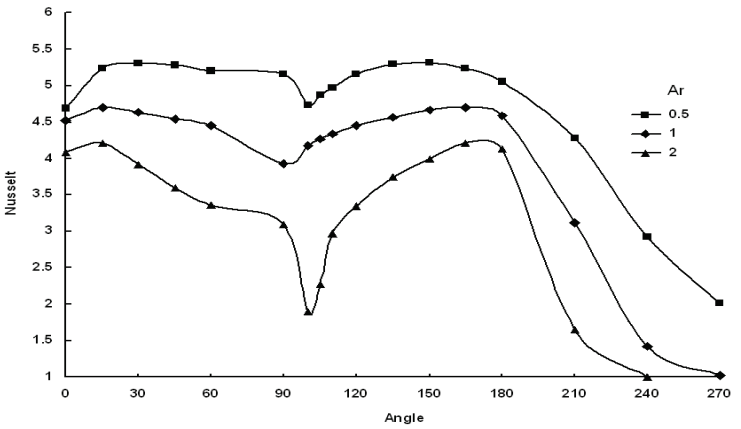

Figure 8: The coupled effects of aspect ratio and inclination on the Nusselt number for Pr=0.71 and $Ra = 10^5$.

4.4 The coupled effects

Previous researches using standard Navier-Stokes solvers tried to establish correlations for Nusselt number as a function of the different parameters cited above (Kerr and Herring (1999)). In this part we are interested in studying the coupled effects

of the inclination and the aspect ratio at the same time on heat transfer. Two aspect ratios 0.5 and 2 are investigated. The results obtained are gathered in Fig. 8 for purpose of comparison.

For Ar=0.5 no change observed in the thermal behavior of flow, the same profile is obtained but quantitatively the Nusselt number increases and the profile is translated due to the conductive effect. However, for Ar=2 the flow becomes periodic at $\gamma = 90^\circ$. The dynamic flow structure changes many times at one period and the dimensionless frequency is close to 15.81. The corresponding time-averaged Nusselt number at the isotherm wall is close to 3.16. The flow is also periodic for $\gamma = 100^\circ$, the dimensionless frequency is 21.93 and the time-averaged Nusselt number is 2.06; the streamlines show a small cell near the hot wall and a great cell near the cold wall, which is three times the small one. At $\gamma = 105^\circ$ the flow is found to be chaotic, however, for $\gamma = 110^\circ$ the flow becomes steady and it remains steady for $\gamma \geq 110^\circ$. The behavior will certainly change if the Rayleigh number values change (see for instance bennacer et al. (2001)).

The effect of the angle of inclination comes to be perceptible with the increase of the aspect ratio. As it is shown in Fig. 8, the heat transfer depends strongly on the aspect ratio. The Nusselt number decreases with the increase of aspect ratio. In the other hand, the coupled effect coming from the increase of the aspect ratio (upper to unit) and the increase of the angle of inclination (upper to 90˚) is expressed by the displacement of angle at minimum and maximum Nusselt number towards the limit 180˚. Note that the best outcome of this part is that for Ar=0.5 (or slightly different), the heat transfer is quasi-independent from the angle of inclination from 15˚ to 90˚.

5 Conclusions and future developments

The problem of natural convection of an incompressible, Boussinesq fluid in a rectangular cavity with differentially heated walls has been investigated numerically. The LBM has been found to be an effective and convenient alternative to simulate laminar flows in confined spaces.

The study has been conducted in three steps.

First, we have presented the LBM as a new tool having good properties such as algebraic operations and accuracy.

Second, we have conducted a comparative study of heat and fluid flow in heated square cavities. The present grid sizes have proven to yield the same order of accuracy as the other solvers. It has been shown that high values of the characteristic number need high grid resolution to get accurate solutions.

Third, the effect of the secondary parameters (geometry, configuration and fluid

properties) on the heat and fluid flows has been considered. The results of the LBM have been found to be in good agreement with earlier works.

We would like to mention that the advantage of the local collision step in LBM is to allow relatively simple implementation on parallel computers.

As shown by Succi (2001), Huidan Yu (2005) and C. Shu 2006), turbulent flows occur at high values of the characteristic number, so boundary layers need grid refinement to be well captured. Here it has been shown that TLLBM recently developed by C. Shu can be used as an efficient tool to handle arbitrary meshes and turbulent regime and to be combined with various models of turbulence.

The next step in our works will be to introduce, first, a grid refinement using the TLLBM approach and, second, a large-eddy modeling of turbulence. The turbulent dissipative effects will be modeled by a new term associated to the molecular viscosity. This term is generally regarded as a turbulent or eddy viscosity appearing in the relaxation time computed from the filtered strain rate tensor in the Smagorinsky model (see Yu, Luo, and Girimaji (2006)).

Acknowledgement: The authors would like to thank Dr. A. A. Mohamad for fruitful comments and discussions during his invited position in the University of Limoges, summer 2008.

References

Bennacer R.; El Ganaoui M.; Leonardi E. (2006): Vertical Bridgman Configuration Heated From Below: 3d Bifurcation And Stability Analysis, *Applied Mathematical Modelling*, 30, (11), pp. 1249-1261,

Bennacer R.; Beji H.; Duval R.; Vasseur P. (2000): The Brinkman Model For Thermosolutal Convection In A Vertical Annular Porous Layer, *Inter. Com. Heat Mass Transfert*, Vol. 27, No 1, 69-80.

Bennacer, R.; Mohamad, A. A.; Sezai, I. (2001): Validation Exercise Natural Convection In Air-Filled Cubical Cavity, 2nd Int. Conf. for Heat Transfer Symposium, CHT-01, Palm Cove, Australia (25-28 Mai, 2001).

Bouali, H.; Mezrhab,A.; Amaoui, H.; Bouzidi, M. (2006): Radiation-natural convection heat transfer in an inclined rectangular enclosure, *Int. J. Thermal Sci.*, 45, pp. 553-566.

Bouzidi, M.; D'Humières, D.; Lallemand, P.; Luo, L. S. (2001): Lattice Boltzmann equation on a two-dimensional rectangular grid, *J. Comput. Phys*. 172, pp. 704-717.

Chen, S.; Doolen, G. D. (1998): Lattice Boltzmann method for fluid flows, *Annu.*

Rev. Fluid Mech., 30, pp. 329-64.

Chew, Y. T.; Niu, X. D. Shu, C. (2006): Three-dimensional lattice Boltzmann BGK model and its application to fows with heat transfer in a rectangular microchannel, *Int. J. Numer. Meth. Fluids*, 50, pp. 1321-1334.

D'Humières, D.; Bouzidi, M.; Lallemand, P. (2001): Thirteen-velocity three-dimensional lattice Boltzmann model, *Phys, Rev. E*, 63, 066702.

de Gassowski, G.; Xin S.; Daube, O. (2003): Bifurcations et solutions multiples en cavité 3D différentiellement chauffée, *C. R. Mécanique*, 331, pp. 705-711.

D'Orazio, A.; Corcione, M.; Cielata G. P. (2004): Application to natural convection enclosed ?ows of a lattice Boltzmann BGK model coupled with a general purpose thermal boundary condition, *Int. J. Thermal Sci*., 43, pp. 575-586.

de Vahl Davis G. (1983): Natural convection of air in a square cavity: A benchmark numerical solutions, *Int. J. Numer. Methods Fluids*, 3, pp. 249-264.

El Ganaoui, M.; Bontoux, P. (1998): An homogenisation method for solid-liquid phase change during directional solidification, ASME, H.T.D., Numerical and Experimental Methods in Heat Transfer, éd. R.A. Nelson, T. Chopin, S.T. Thynell, vol.361(5), 453-469.

El Ganaoui, M. (2002): Computational Modeling of heat mass and solute transport in solid/liquid transition systems on earth and on microgravity environment. Mecanica Computational vol XXI, ISSN 1666-6070, Eds. S. R. Idelsohn, V. Sonzogi, A. Cardona, p. 2587-2592.

El Ganaoui M., Prud'homme (2004): R. Editors, Microgravity and transfers, spécial issue Comptes Rendus Mécanique, Volume 332, Issues 5-6.

Filippova, O.; Hanel, D. (2000): Acceleration of Lattice-BGK Schemes with Grid Re?nement, *Journal of Computational Physics*, 165, pp. 407-427.

Guo, Z.; Shi, B.; Zheng, C. (2002): A coupled lattice BGK model for the Boussinesq equations; *Int. J. Numer. Meth. Fluids*, 39, pp. 325-342.

Guo, Z.; Zhao, T. S. (2003): Explicit ?nite-difference lattice Boltzmann method for curvilinear coordinates, *Physical Review E*, 67, 066709.

Guo, Z.; Zhao, T. S. (2005): A Lattice Boltzmann model for convection heat transfer in porous media; *Numerical Heat Transfer, Part B*, 47: pp. 157-177.

He, X.; Chen, S.; Doolen, G. D. (1998): A novel thermal model for the lattice Boltzmann method in incompressible limit, *Journal of Computational Physics*, 146, pp. 282-300.

He, X.; Luo, L. S. (1997): Lattice Boltzmann Model for the Incompressible Navier-Stokes Equation; *Journal of Statistical Physics*, Vol. 88, Nos. 3/4, pp. 927-944.

He, X.; Zou, Q.; Luo, L. S.; Dembo, M. (1997): Analytic Solutions of Simple Flows and Analysis of Nonslip Boundary Conditions for the Lattice Boltzmann BGK Model, *Journal of Statistical Physics*, Vol. 87, Nos. 1/2, pp. 115-136.

Hou, S.; Zou, Q. (1995): Simulation of cavity flow by the Lattice Boltzmann method, *Journal of Computational Physics*, 118, pp. 329-347.

Ismail, K.A.R.; Scalon, V. L. (2000): A ?nite element free convection model for the side wall heated cavity, *Int. J. Heat Mass Transfer*, 43, pp. 1373-1389.

Jami, M.; Mezrhab, A.; Bouzidi, M.; Lallemand, P. (2007): Lattice Boltzmann method applied to the laminar natural convection in an enclosure with a heat-generating cylinder conducting body, *Int. J. Thermal Sci*., 46, pp. 38-47.

Jami, M.; Amraqui, S. Mezrhab, A.; Abid, C. (2008): Numerical study of natural convection in a cavity of high aspect ratio by using the lattice Boltzmann method, *Int. J. Numer. Meth. Engng*, 73, pp. 1727-1738.

Kerr, R. M.; Herring, J. R. (1999): Prandtl number dependence of Nusselt number in DNS, *J. Fluid Mech.*, vol., (22 pp.).

Lallemand, P.; Luo, L. S. (2003): Lattice . Boltzmann method for moving boundaries, *Journal of Computational Physics*, 184, pp. 406-421.

Lappa M., (2007). Secondary and oscillatory gravitational instabilities in canonical three-dimensional models of crystal growth from the melt, special issue comptes rendues de mécanique, Editors M. El Ganaoui, R. Prud'homme, R. Bennacer, 261-268.

Massaioli, F.; Benzi, R.; Succi, S. (1993): Exponential tails in two-dimensional Rayleigh-Bénard convection, *Europhys. Lett.*, 21 (3) 305.

Mohamad, A. A. (2007): Applied Lattice Boltzmann Method for Transport Phenomena, Momentum, Heat and Mass Transfer, (Book).

Mezrhab, A.; Bouzidi, M.; Lallemand, P. (2004): Hybrid lattice-Boltzmann finite-difference simulation of convective ?ows, *Computers & Fluids*, 33, pp. 623-641.

Mezrhab, A.; Jami, M.; Abid, C.; Bouzidi, M., Lallemand, P. (2006): Lattice-Boltzmann modelling of natural convection in an inclined square enclosure with partitions attached to its cold wall, *Int. J. Heat and Fluid Flow*, 27, pp.456-465.

Mezrhab, A.; Jami, M.; Bouzidi, M.; Lallemand, P. (2007): Analysis of radiation-natural convection in a divided enclosure using the lattice Boltzmann method, *Computers & Fluids*, 36, pp.423-434.

Mezrhab, A.; Moussaoui, M. A.; Naji, H. (2008): Lattice Boltzmann simulation of surface radiation and natural convection in a square cavity with an inner cylinder, *J. Phys. D: Appl. Phys.*, 41, 115502 (17pp).

Mohamad A.A., Bennacer R., Azaiez J., (2004): Double Diffusion Natural Convection In A Rectangular Enclosure Filled With Binary Fluid Saturated Porous Media: The Effect Of Lateral Aspect Ratio, Physics Of Fluids, 16, (1) 184-195.

Ozoe, H.; Sayama, H. (1975): Natural convection in an inclined rectangular channel at various aspect ratios and angles-Experimental measurements, *Int. J. Heat Mass transfer*, Vol. 18, pp. 1425-1431.

Paolucci, S.; Chennoweth, D. R. (1989): Transition to chaos in a differentially heated vertical cavity, *J. Fluid Mech.*, WOE. 201, pp. 379-410.

Peng, Y.; Shu, C.; Chew, Y.T. (2003): Simpli?ed thermal lattice Boltzmann model for incompressible thermal ?ows, *Phys. Rev. ,E*, 68 (026701), pp.1-8.

Qian, Y. H.; D'Humieres, D.; Lallemand, P. (1992): Lattice BGK Models for Navier-Stokes Equation, *Europhys. Lett.*, 17, (6), pp. 479-484.

Semma, E.; El Ganaoui M.; Bennacer R. (2007): Lattice Boltzmann method for melting/solidi?cation problems, *C. R. Mécanique*, 335, pp. 295-303.

Semma, E.; El Ganaoui; Bennacer,M. R.; Mohamad, A. A. (2008): Investigation of ?ows in solidi?cation by using the lattice Boltzmann method, *International Journal of Thermal Sciences*, 47, pp. 201-208.

Vahala, G.; Pavlo, P.; Linda, V; Martys, N. S. (1998): Thermal Lattice Boltzmann Model (TLBM) for compressible flows, *International Journal for Modern Physics C*, Vol. 9, No. 8, pp. 1247-1261.

Yamamotoa, K.; Takada, N.; Misawa, M. (2005): Combustion simulation with Lattice Boltzmann method in a three-dimensional porous structure, *Proceedings of the Combustion Institut*, 30, pp. 1509-1515.

Yu, H.; Luo, L. S.; Girimaji, S. S. (2006): LES of turbulent square jet ?ow using an MRT lattice Boltzmann model, *Computers & Fluids*, 35, pp. 957-965.

Zou, Q.; He X. (1997): On pressure and velocity boundary conditions for the lattice Boltzmann BGK model, *Phys. Fluids*, Vol. 9, No. 6, pp. 1591-1598.